IOP Conference Series: Earth and Environmental Science

PAPER • **OPEN ACCESS**

Microseismic and Focal Mechanism Analyses for Structural Interpretation – Muara Laboh Geothermal Field

To cite this article: Djoko A. Wibowo *et al* 2022 *IOP Conf. Ser.: Earth Environ. Sci.* **1014** 012004

Microseismic and Focal Mechanism Analyses for Structural Interpretation – Muara Laboh Geothermal Field

Djoko A. Wibowo[1], Irvan Ramadhan[2], Indra Agoes Nugroho[2], Marino C. Baroek[2], Novi Ganefianto[2], Herwin Azis[2], Suryantini[3], David P. Sahara[3], and Prima W. Mozef[3]

[1]Geothermal Master Program, FTTM, ITB, Jakarta, Indonesia
[2]PT Supreme Energy Muara Laboh, Menara Sentraya, 23rd floor, Jakarta 12160, Indonesia
[3]Institut Teknologi Bandung, Jl. Ganesa No. 10, Bandung, Jawa Barat, Indonesia

Email: djokoawibowo@gmail.com
https://orcid.org/0000-0002-2205-3352

Abstract. Microseismic monitoring has been used for gathering subsurface information in Geothermal field as part of reservoir monitoring and management plan. New micro earthquake (MEQ) stations were installed in the Muara Laboh geothermal field in the end of 2019, coinciding with the first operation of Unit-1. They have been continuously used to monitor the MEQ events until now. This paper discusses MEQ data analyses to support the subsurface structural interpretation in the Muara Laboh geothermal field. Geothermal production and injection activities create micro seismicity which is triggered by stress failure in fractures / fault planes due to percolation of fluid within fractures network. Distribution of hypocenter locations and magnitude are analyzed, considering highly operational activities, rock mechanic and slip orientation. There are two micro seismicity clusters observed, namely South and North clusters. The South cluster represents 80% of the total recorded micro seismicity events, having NE – SW trend direction; while the North cluster consists of 10% of the total events, correlated with the NNW – SSE structural trend direction. Focal mechanism analysis explains that micro seismicity observed on extended fault zone in the south is thought to be correlated with the distributed fractured network on the hanging wall of normal fault. It is shown by some micro seismicity swarms identified in the south basin-sidewall fault area. These orientations support the current kinematic model of the Muara Laboh geothermal field derived from the structural geology mapping and borehole image logs.

1. Introduction

The Muara Laboh geothermal field is located about 126 km southwest of Padang, the capitol of West Sumatra Province, Indonesia (Figure 1). This paper discusses microseismic monitoring results conducted in the Muara Laboh geothermal field since the start of Plant operation in 2019. New 15 micro earthquake (MEQ) stations were installed in the Muara Laboh field in the end of 2019, coinciding with the start-up of the Muara Laboh Unit-1. They have been continuously used to monitor the MEQ events until now. This study uses MEQ data from one-year period between November 2019 to November 2020.

MEQ data was processed through a robust data processing and waveforms picking QA/QC. A total of 704 microseismic events identified, which 636 of them were successfully picked with total of 3002

P-wave arrival time and 3008 S-wave arrival time. The accuracy of the hypocenter locations has been improved by using hypocenter relocation double-differential method and was further improved by applying waveform cross-correlation (WCC) technique.

The Muara Laboh geothermal resource is indicated by the presence of thermal manifestations consisting of fumaroles, hot springs, mud pools, and steaming grounds which discharge along structures associated with the Great Sumatran Fault near young volcanic centers such as Patah Sembilan volcanic center (Figure 2).

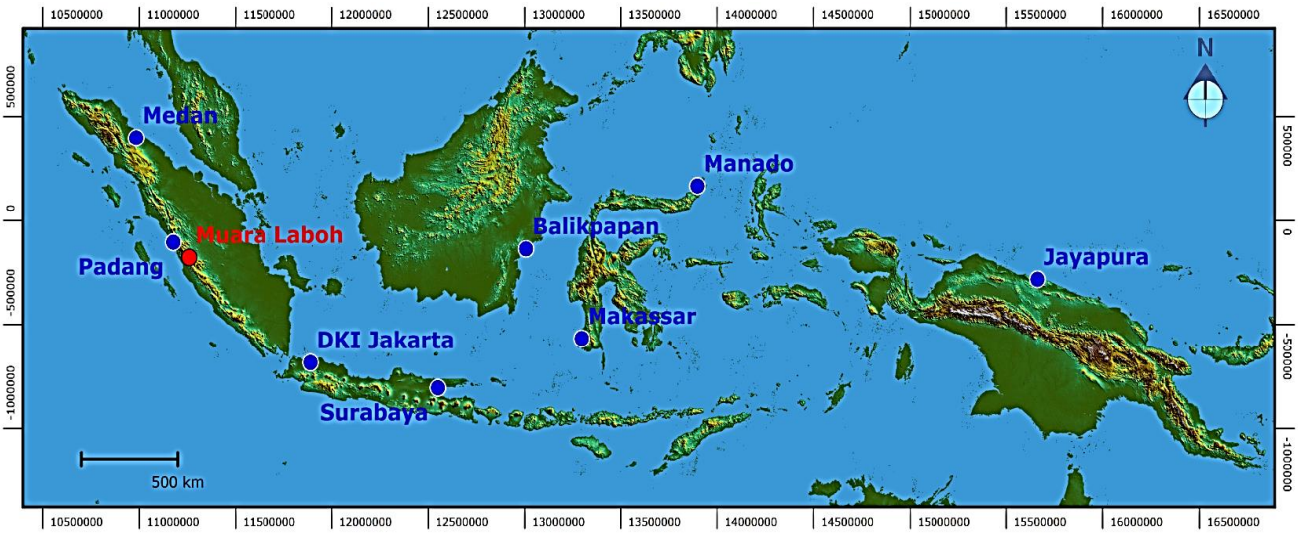

Figure 1. Muara Laboh geothermal field location in West Sumatra Province, Indonesia, and its relative position to Jakarta and Padang cities.

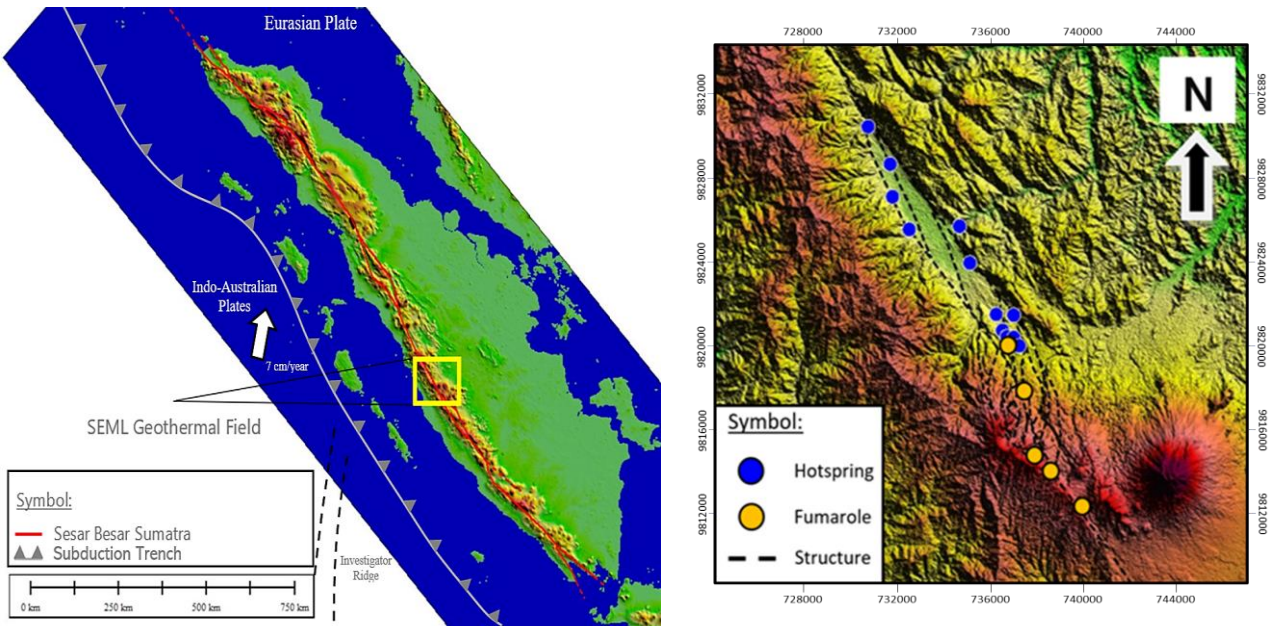

Figure 2. Left: Location of Muara Laboh geothermal field related to the Great Sumatran Fault (GSF). Right: Thermal manifestations distribution in Muara Laboh (modified after [1]).

2. Geology and Tectonic Setting

Tectonic evidence of Sumatra Island is constructed by extensive right-lateral strike-slip fault that extends 1,900 km over northern part of the island in Banda Aceh, NAD province to southern part of the island in Kota Agung, Lampung. This strike slip fault is known as the Great Sumatran Fault (GSF) which is divided into 19 segments [2] based on major local changes in strike-slip fault behaviour. Discontinuities of these strike-slip segments are right steps and thus result a dilatational step over. This dilatational step over is theoretically large enough to influence the seismic behaviour of the fault [3][4] that have distinct the pattern of seismicity in each segment. There are 13 pull-a-part basins that has been defined in the GSF dilatational step overs [5].

Volcanism in Sumatra Island occurs within 10 km of GSF [6]. The pair of GSF and recent volcanism in Sumatra Island has encouraged numerous of high-temperature geothermal systems. Muara Laboh is one of the examples which is formed inside the pull a part basin of a right-stepovers GSF segment, between the Suliti and Siulak faults. Many other Sumatran geothermal systems are located along or near the GSF, both inside the pull a part basin or along the extensional fractures of the main or subsidiary faults [7][8].

Geologically, the Muara Laboh geothermal field sited in a pull-a-part setting controlled by dextral strike-slip GSF fault segments of Siulak and Suliti [1]. The field is situated on the slopes of the volcanic edifices of Mt. Bangko, Mt. Anak Patah Sembilan, Mt Patah Sembilan and Mt. Kapur. The biggest volcano near the SEML geothermal field is Mt. Kerinci which volcanically active, type A, 100 km Southeast of the geothermal field according to Pusat Vulkanologi dan Mitigasi Bencana Geologi [9].

The stratigraphy of Muara Laboh consists of pre-Tertiary basement rock which is overlaid by volcanics intrusion and Tertiary sediments rock [1]. The oldest rock of Muara Laboh geothermal field is Paleozoic Barisan Formation (Pb) with composition of metamorphic rock, and marble (Pbl). Above the Paleozoic Barisan Formation, overlies the Siguntur Formation (Ps) and Cretaceous Granit intrusion (Kgr). Tertiary mixed volcanic and sedimentary rock then overlies Pre-Tertiary basement, unconformably, to forms Painan Formation (Tomp), and granitic (Tgr), granodioritic (Tgdr) rock that intruded the Barisan and Painan Formations.

Undifferentiated Silicic Volcanic rocks (Qou and Qol) are distributed in the northwest, west and southwest of Muara Laboh field. These volcanic products are 1000 m thickness according to exploration wells data. Those are underlying recent andesitic rock (Qyu) which were erupted to the southeast of Muara Laboh and filled the basin with basaltic to andesitic lava, and pyroclastic products, such as lahars, volcanic sediment, fluvial deposit and lacustrine sediment and detritus of marine sediment. These volcanic products and sediments are mixed and intercalated inside Muara Laboh basin.

The last young Quaternary volcanics are deposited above the Qou, Qol and Qyu formations, as a product of Mt. Bangko (Qb), Mt. Patah Sembilan (Qps), Mt. Anak Patah Sembilan (Qaps), Mt. Kapur (Qk), and Mt Kerinci volcanic centre (Qyl). These volcanic and sedimentary products generally deposited following the hydrology pattern from the eruption center along the Siulak fault in the south towards north. The distal area deposits are dominantly arranged by volcaniclastic of the eruptive products. Details of Muara Laboh stratigraphy is shown in Figure 3 below.

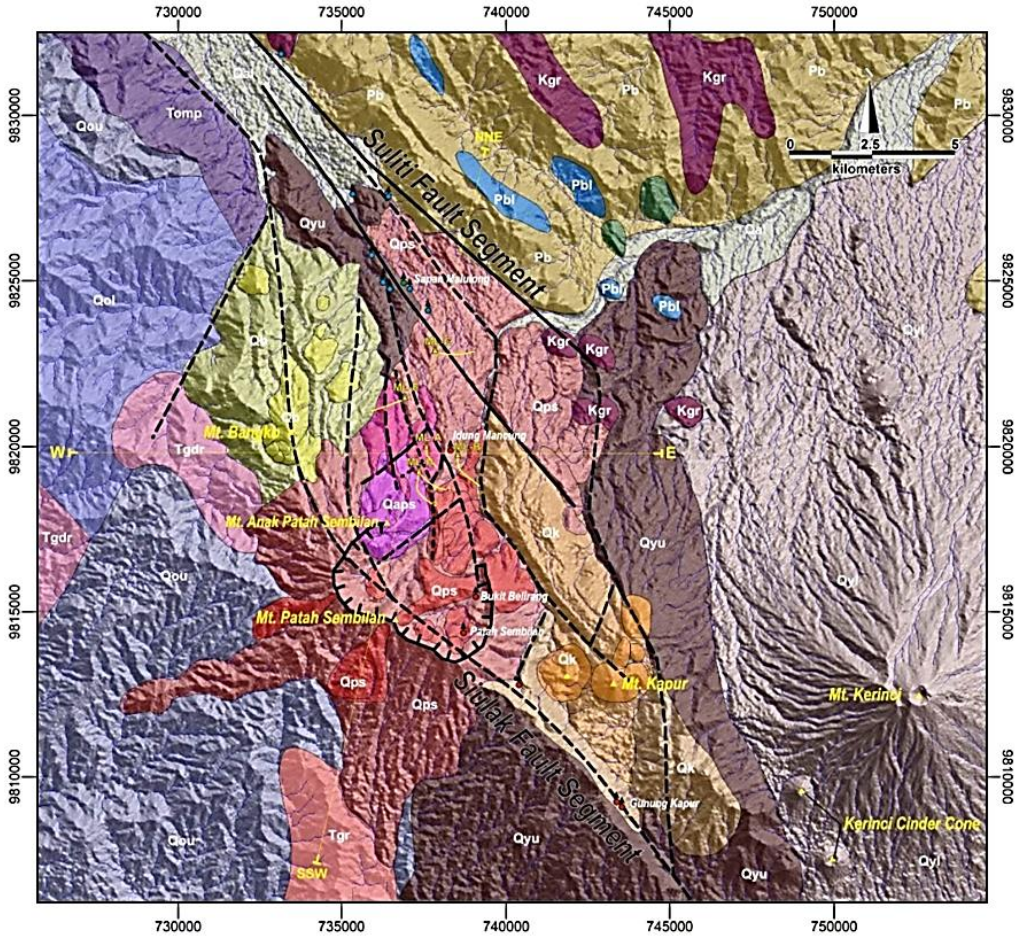

Reference Ages	Regional Tectonic Stratigraphic Stages	Volcanic & Sediment / Intrusive	Formation/ Volcanic Product & Lithology	Geohistorical Stratigraphy & Fault Structure	Stratigraphy & Geothermal System
Quaternary (*<1.8 Ma*)	ACTIVE VOLCANISM AND BASINAL IN-FILLING BY VOLCANIC PRODUCTS Reactivation-Continuity Active GSF	Qal Qyl Qaps Qps Qb Qk Seds Qyu Qou/l	Aluvium Mt. Kerinci Mt. Kapur Mt. Anak Patah Sembilan Mt. Patah Sembilan Mt. Bangko Undifferentiated silicic volcanic rocks Andesite volcanic rocks and Intercalation andesite & silicic	Recent alluvium actively filling the valley and river plain. Mt. Patah Sembilan, Kapur & Kerinci volcanic complexes and with andesitic composition sequence of tuffs, breccia and lava. Silicic (dacite to rhyolitic) sequence (Qou/l) dominated by tuffs but including lava and volcaniclastic units. Andesitic volcanic sequence (Qyu). Products dominated by lava, pyroclastic, and associated volcanic sediment & sediment. Intercalated with silicic volcanic sequence. *Step-over initiates local depocentre formation (right lateral dextral strike slip).*	Hosts Reservoir Clay Cap Shallow Reservoir Intermediate Zone
Tertiary (Oligocene to Miocene *33-5.3 Ma*)	HORST AND GRABEN STAGE GSF start active faulting	Tgdr Tgr Tomp	**Granite & Granodiorite** **Painan Formation:** Volcanic (andesitic to silicic) & Sedimentary (shale to sandstone)	**Unconformity** - uplift exposes granite & granodiorite to surface. Initiation of GSF in mid-Miocene (13 Ma) (Barber et al., 2005 and references therein). Magmatic arc granites & granodiorites (Tgr & Tgdr) intruded, within horse and graben structures. Tertiary lava, pyroclastic, volcaniclastic, and sedimentary deposits (Tomp) fill the horse and graben system. *Faulting of the Pre-Tertiary rocks creates horse and graben system (extension).*	Deep Reservoir
Mesozoic (Cretaceous *144 Ma*)	PRE-RIFT Final stage of stable craton	Ps Kgr	**Granitic Rocks** **Siguntur Formation:** Quarzite	**Unconformity** - Pre-Tertiary rocks are uplifted, folded, and faulted, with local metasomatism (McCarthy & Elders, 2014.) Intra-continent sedimentation (Ps) while the granites (Kgr) intruded the Paleozoic rocks.	Outside Reservoir
Paleozoic (Permian *248 Ma*)		Pbl Pb	**Bukit Barisan Formation:** Phyllite, slate, limestone, metagreywacke	**Unconformity** - uplift and erosion. Offshore deposition, burial and metamorphism.	

Figure 3. Stratigraphy and geology map of Muara Laboh [1].

3. Microseismic Monitoring and Data Processing

Microseismic is a low-magnitude seismicity (M < 2) [10] which is usually being monitored while fluid is injected into geothermal reservoir or during production phase [11][12]. Microseismic can also be associated to volcanic activity where the fluid moves from the earth crust to surface [13]. Microseismic monitoring is commonly conducted on operated geothermal field to recognize fracture activity due to fluid movement on the local region [10]. Microseismic can also happen because of the change (disrupt) of rock stress distribution. When the rock body redistribute the stress, slip or shear will happen [10]. This process leads to the making of fault.

The distinct characteristic of microseismic are: the frequency ranged between 2 to 50 Hz (in some occasion could reach 300 Hz); have small moment magnitude (under 3); and the P- and S- wave arrival time difference is lower than 3 seconds. The important job on microseismic monitoring is classifying the recorded signal type into several class, for instances microseismic, regional earthquake, or teleseismic earthquake. After classifying the event type, then data processing is performed to determine the hypocenter location of the corresponding microseismic. The determination of P and S wave arrival time plays an important role on hypocenter quality. To elevate the quality of P and S wave arrival time determination, we can use filtering, wadati diagram analysis, and waveform cross-correlation [14].

Seismometer station for microseismic monitoring is equipped with GPS in order to get geographical coordinate and timestamp from the satellite on continuous mode. The coordinate information will later be analyzed to determine the more robust location of the corresponding stations (Figure 4).

Initial microseismic event is performed automatically using the filter picker algorithm [15][16]. All identified event will then be evaluated manually, and arrival time determination is performed using the processing software. Microseismic identification and arrival time determination is cautiously performed using manual vision. To control the quality of arrival time determination, we used Wadati diagram to compare the determined Vp/Vs and regional Vp/Vs as the reference where it should be valued near 1.73.

To increase the accuracy in determining arrival time, it carried out waveform cross-correlation method since arrival time picking can have error caused by human errors. Correlation was performed between master event and pair event to see the similarity between master event and pair event, with similar events have high correlation coefficient, in this case, significant correlation coefficient is 0.7 – 1.0. The output will give the best lag time for those pairs. Next, wave arrival time will be corrected based on those lag times. For each station, a master event with the highest signal-to-noise ratio is chosen. The master event will be cross correlated with each event from the station. This process is iterated for every stations. Obtained arrival time correction in from each event pair will be used as input in double-difference method.

Double difference is a method in determining the position of the earthquake hypocenter that uses data from the travel time between earthquake pairs to a seismic station [17]. This method uses the principle that if the distance between two paired earthquakes is relatively smaller than the distance between the seismic stations to each paired earthquake, the ray path and waveform can be considered from one source [17]. This method will minimize the residual time from the calculated travel time and the observed travel time for the earthquake pairs between the same seismic stations (Figure 5).

Double difference hypocenter relocation process is done with required inputs 1D velocity model, event catalog data and phase of wave arrival time, and seismic stations coordinate. From several models, the minimum root mean square (RMS) error and distribution pattern that matches the criteria is selected.

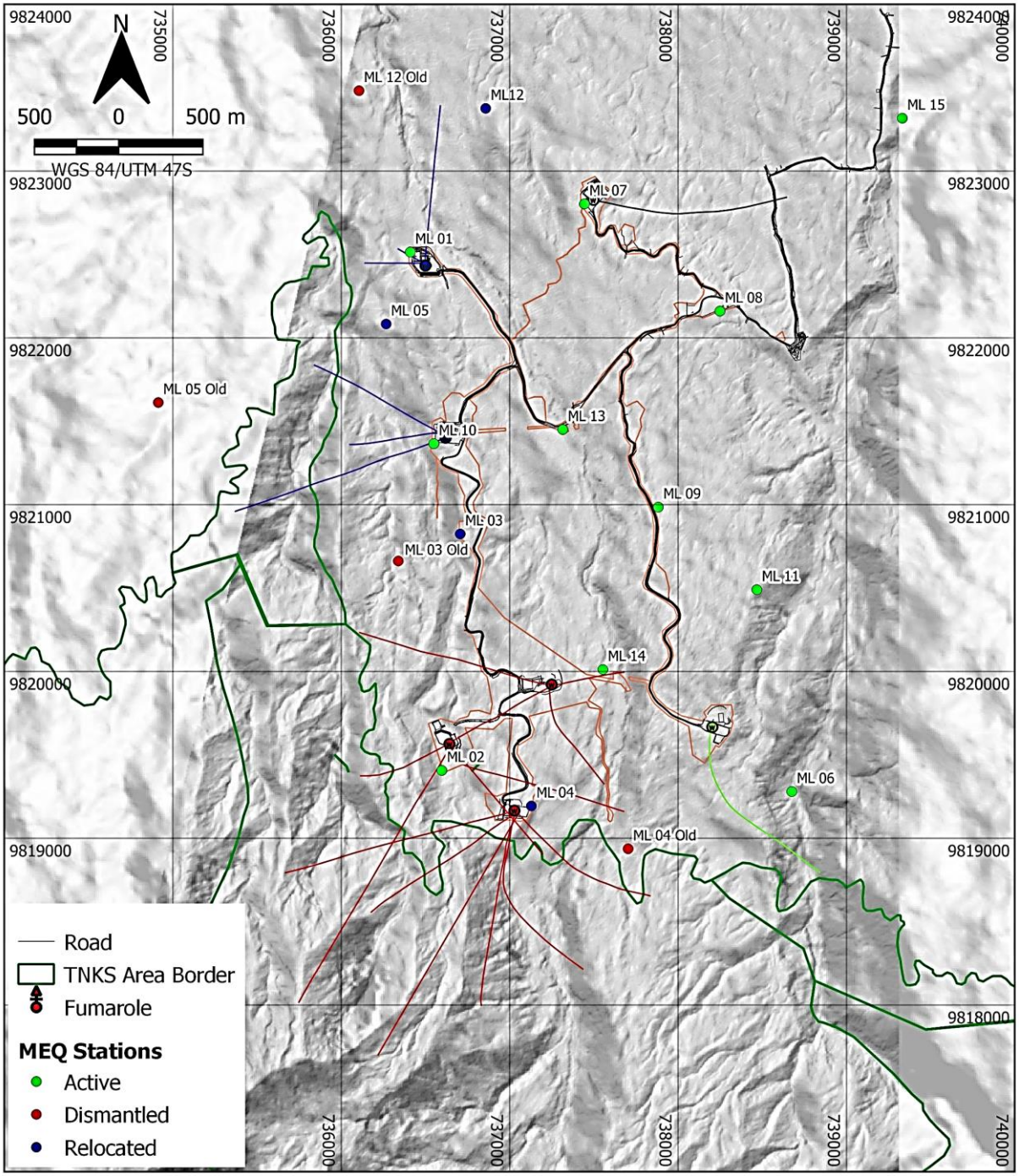

Figure 4. Distribution map of 15 seismometer stations and wells trajectories in Muara Laboh geothermal field.

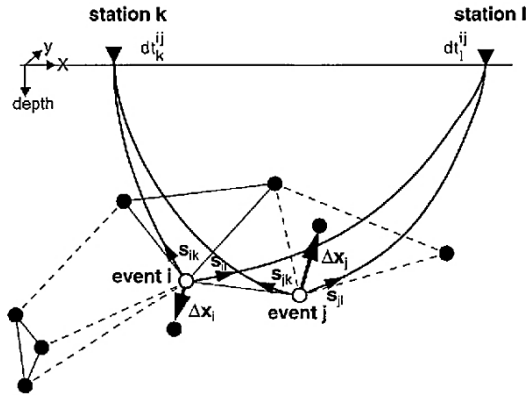

Figure 5. Illustration of hypocenter relocation with double-difference method [17].

4. Microseismic Events Distribution

Initial event location was successfully determined and located mostly south outside of the station networks (GAP > 180). Total amount of 636 events were located very local and small magnitude (M<2). Most of them were detected by 4 monitoring stations. Double difference without waveform cross correlation (WCC) had successfully relocated 509 events, while double difference with waveform cross correlation (WCC) had successfully relocated 408 events. The difference time of 39,346 pair events have been improved using waveform cross correlation (WCC) technique. They are corrected by less than 0.1 s for about 80% of the event pairs. Combination of WCC and DD could reduce the RMS residuals to around 0.02 s, which corresponds to around 100 m event uncertainty.

Microseismic epicenters from one-year period monitoring can be seen in Figure 6 below. These microseismic epicenters are double difference relocation with WCC. Production and injection well are shown distinctly with wellpad name. RMS comparison shows that double difference relocation with WCC has lowest RMS value (it is shown in Figure 7).

There are two microseismic clusters observed, namely North cluster (in blue circle) and South cluster (in red circle). North cluster consists of 10% events, South cluster consists of 80% events, and another 10% is disseminated around monitoring area. These MEQ events are located in a depth ranging from 0 to -2000 masl. Microseismic events distribution in both clusters are aligned with structure trends indicating that the events are correlated with these structures.

5. Moment Magnitude Calculation

To get moment magnitude (Mw), all recorded data on all stations in the monitoring area are used. Radiation pattern correction use averages of the absolute value, where the correction for P-wave is 0.44 and for S-wave is 0.60 [18]. Radiation pattern correction value is an important factor that affects Mw calculation results. The use of average correction can give a maximum difference of 0.8 points [19]. The use of average correction has a tendency to give an overestimated or underestimated Mw, with opposite effects on P-wave and S-wave. Therefore, P-wave and S-wave are calculated independently and evaluate the average value of correction. This method can compensate the error that results from the other one [20].

Moment magnitude is the average of all stations to ensure small variance between stations, so it is expected to get more accurate moment magnitude. Magnitude of completeness in Muara Laboh geothermal field is on Mw 0 (Figure 8). Moment magnitude distribution for all events is shown in Figure 8 with circle's scale and color illustrate the magnitude of each event.

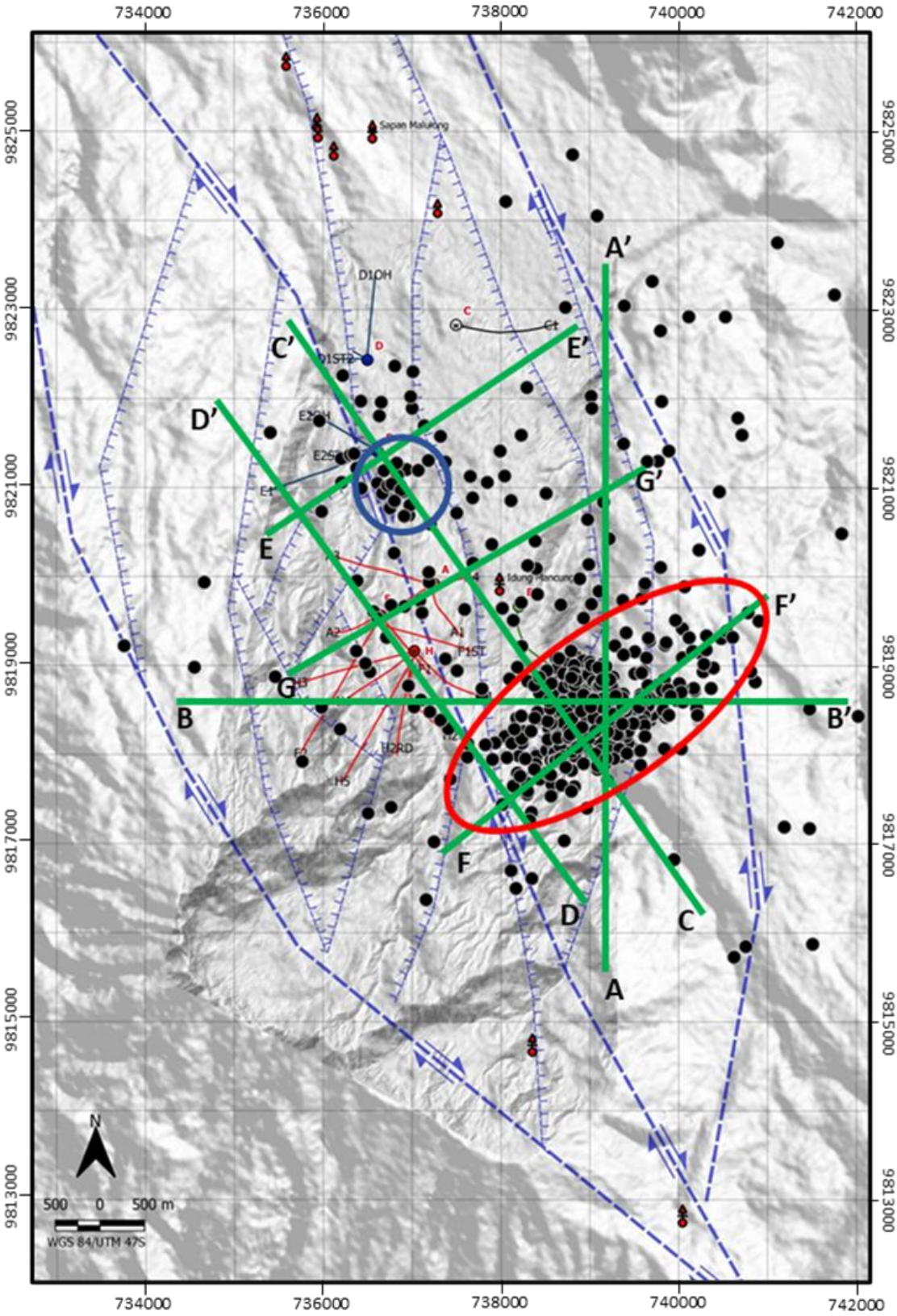
734000
736000
738000
740000
742000
9825000
9823000
9821000
9819000
9817000
9815000
9813000
Sapan Malukang
D1OH
D1STR
C
C1
A'
C'
E'
D'
E2OH
E2ST
E1
G'
E
F'
A2
A1
P1ST
G
B
B'
H2RD
H5
F
D
C
A
N
500 0 500 m
WGS 84/UTM 47S

(a)

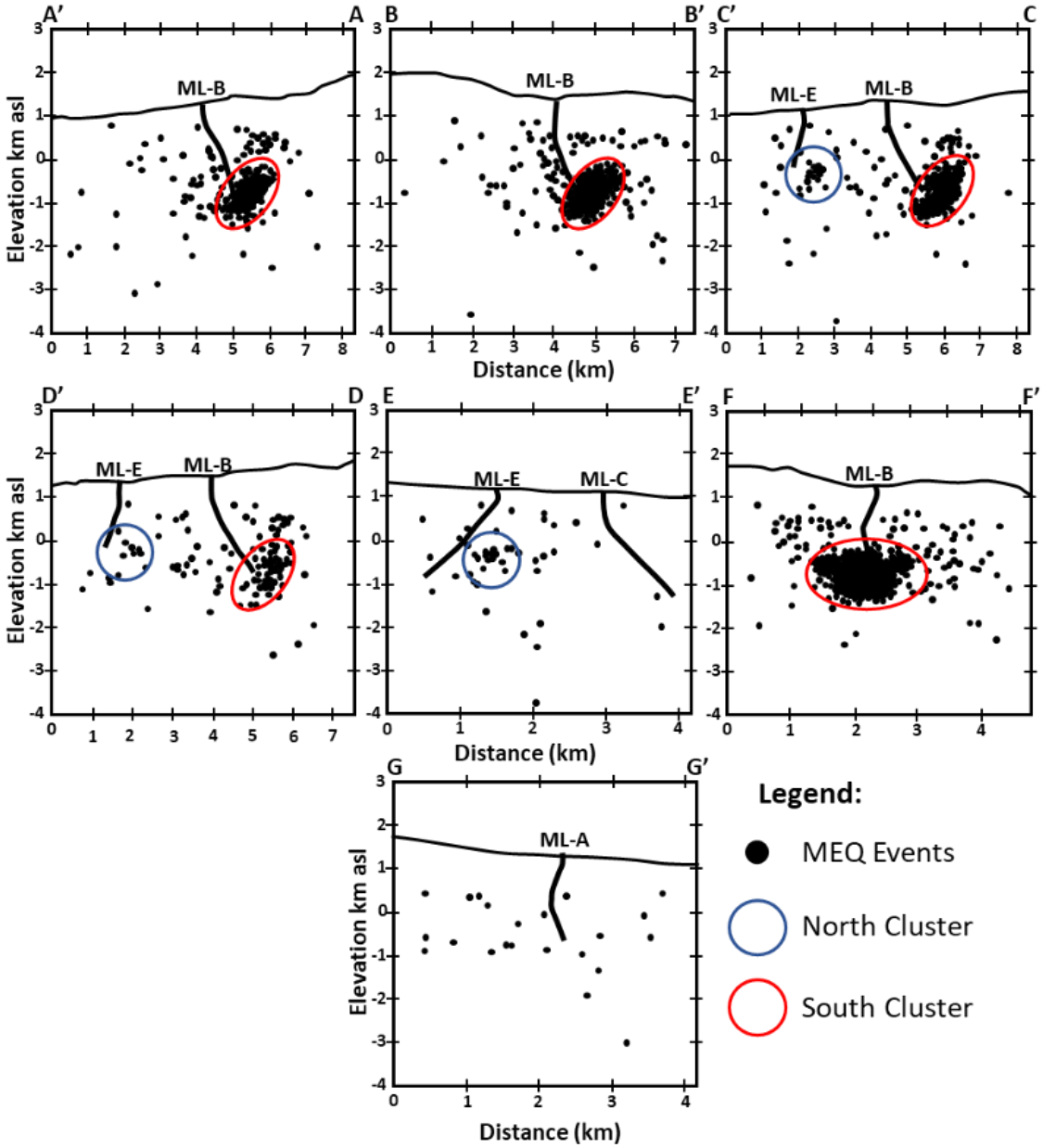

(b)

Figure 6. (a) Map showing distribution of microseismic overlain on structure map [21] and (b) cross sections of microseismic distribution from November 2019 to November 2020.

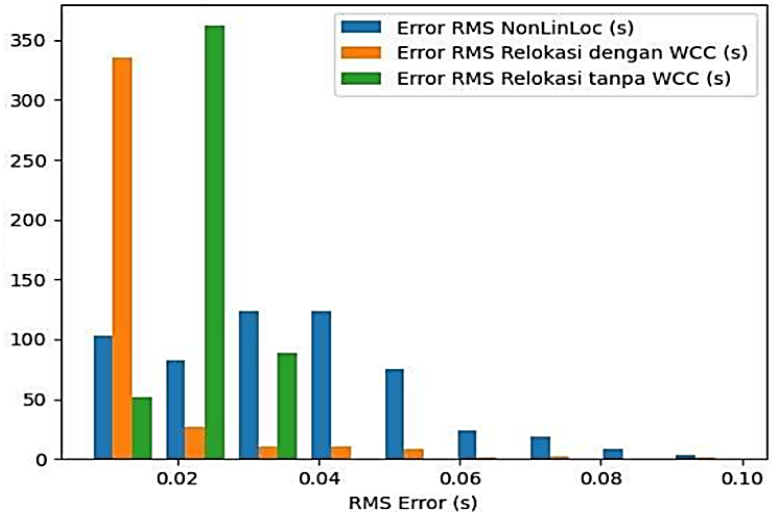

Figure 7. RMS comparison histogram between stages.

6. Focal Mechanism

Focal mechanism shows the orientation of fault plane and the slip on fault plane relative to geographic coordinates. Focal mechanism is one of the most important parameters to define after hypocenter locations. This parameter is used to determine actual geometry of the fault plane and estimate the force and stress of the fault in a region. Focal mechanism solutions can be estimated well when the stations are pretty close from each other, velocity model have been defined, and P-wave first arrival record is clear.

From total 636 microseismic events, at least 10 focal mechanism solutions with standard deviation less than 20° are selected. 5 focal mechanism solutions are taken from North cluster and 5 focal mechanism solutions are taken from South cluster. Focal mechanism inversion result shows that the events on North cluster dominantly controlled by strike slip with oblique dip slip mechanism (Figure 9). While on South cluster, microseismic events are dominantly controlled by normal fault mechanism with one outlier indicating thrust fault mechanism. The focal mechanism data is consistent and support the updated subsurface structural interpretation [21]. Vertical sections of focal mechanism solution in Muara Laboh can be seen in Figure 10.

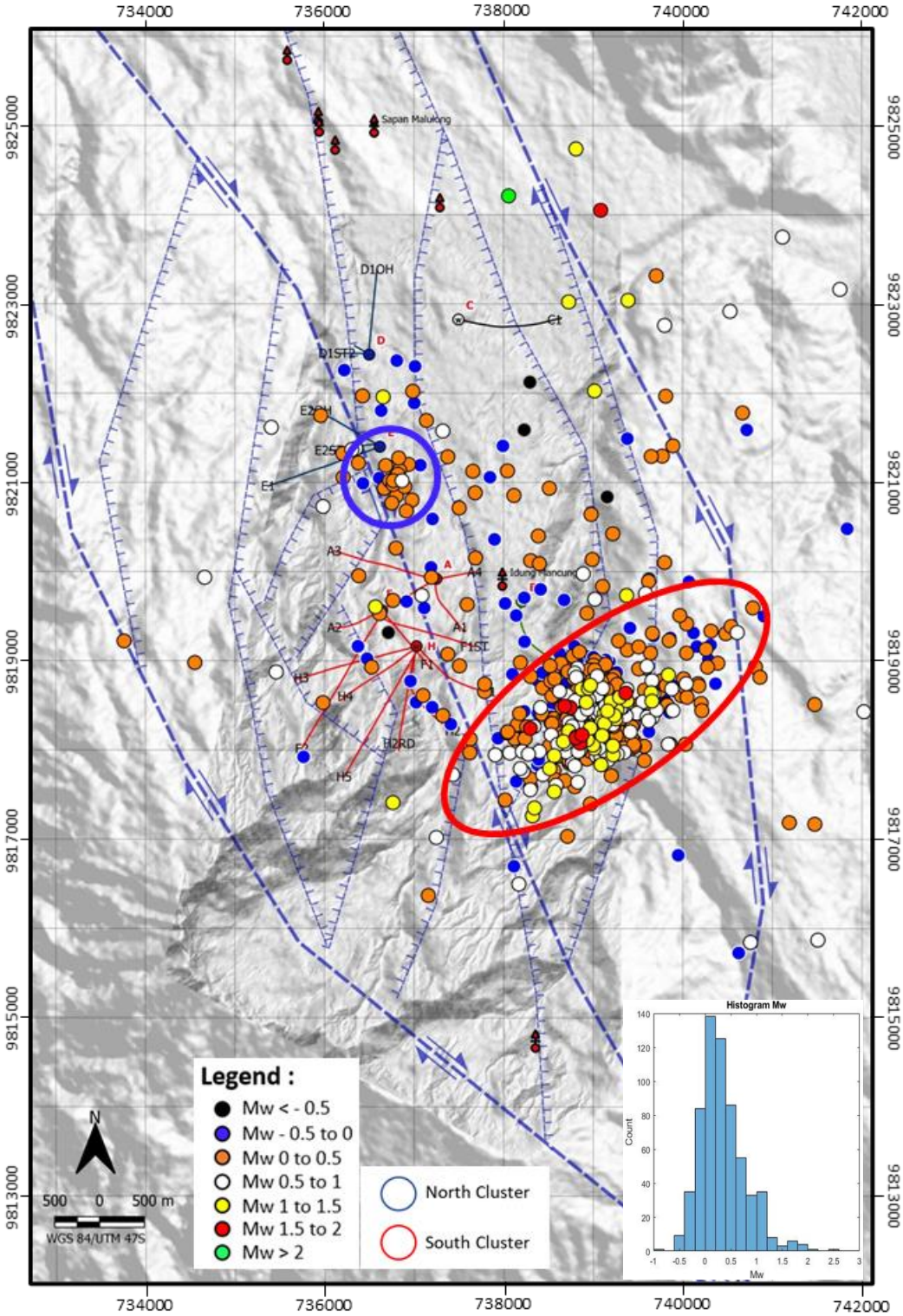

Figure 8. Moment magnitude (Mw) distribution map for microseismic events and histogram for moment magnitude for all events with magnitude of completeness at Mw 0.

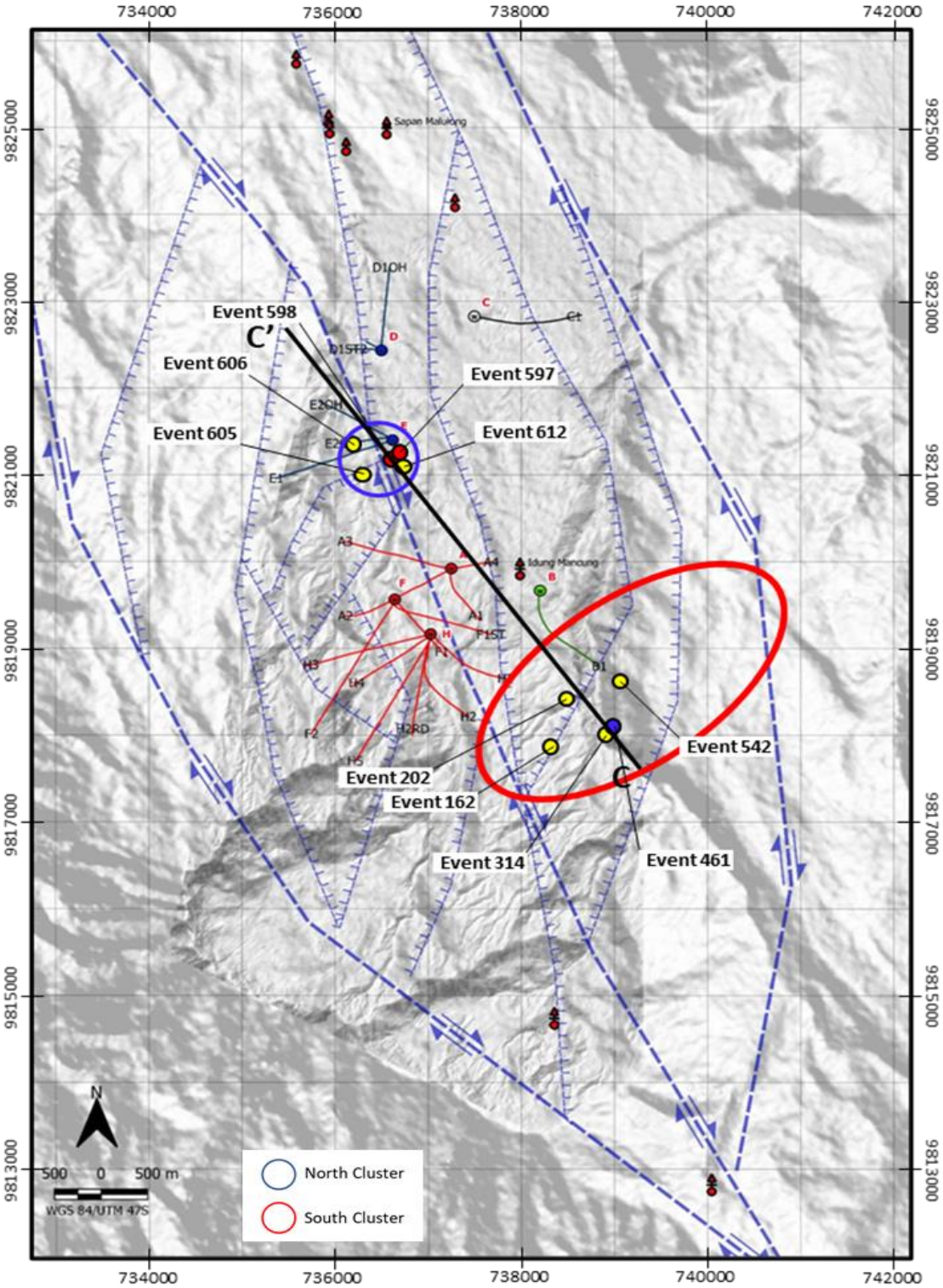
734000
736000
738000
740000
742000
9825000
9823000
9821000
9819000
9817000
9815000
9813000
Sapan Maluong
D1OH
D1ST2
D
C
C1
Event 598
C'
Event 606
Event 597
E2OH
Event 605
Event 612
E2
E1
F
A3
A
A4
Idung Mancung
B
A2
A1
P1ST
H
H1
H3
H4
H
B1
H2
F2
H2RD
H5
Event 542
Event 202
Event 162
C
Event 314
Event 461
N
500 0 500 m
WGS 84/UTM 47S
North Cluster
South Cluster

(a)

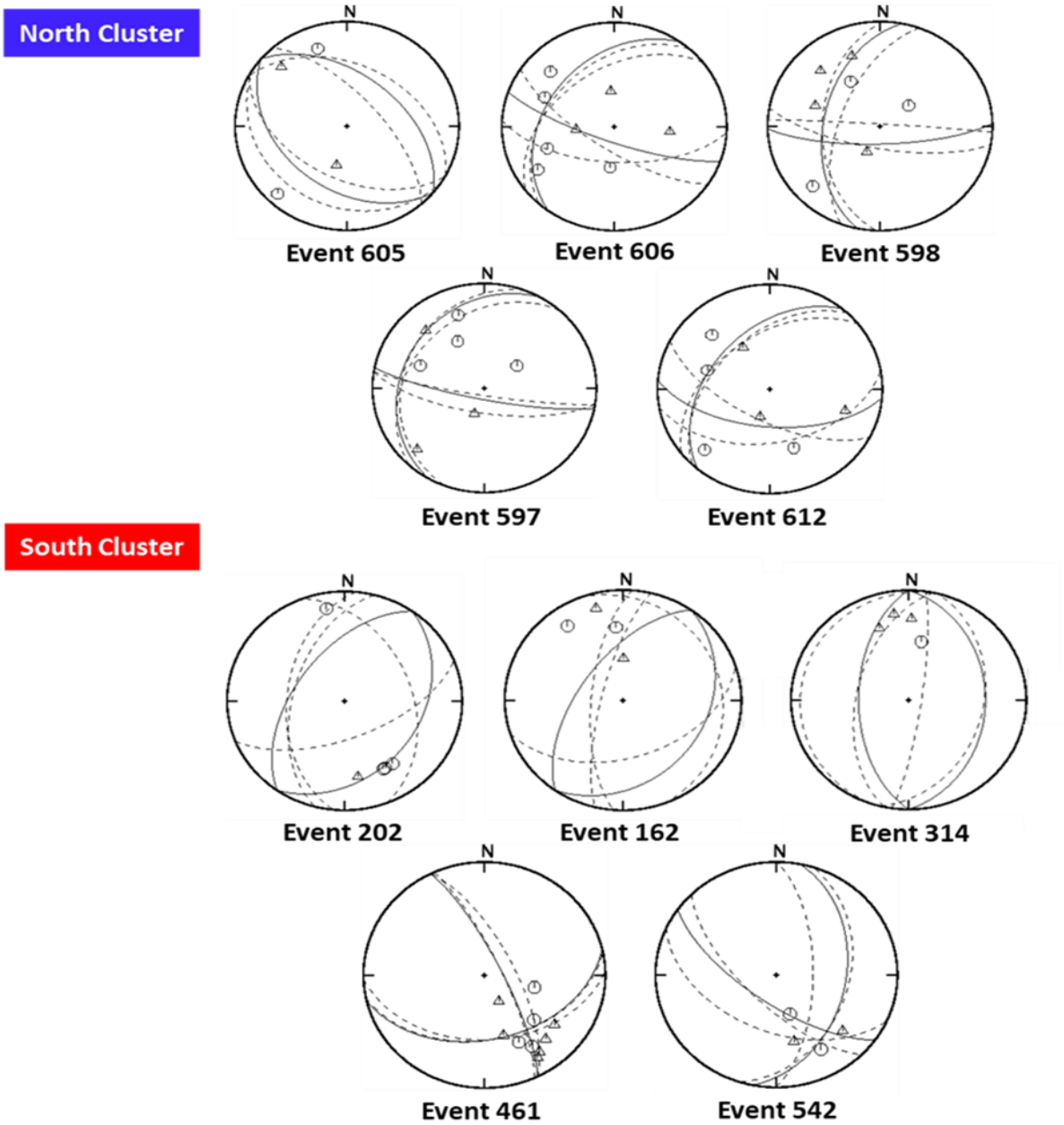

(b)

Figure 9. (a) MEQ Events with focal mechanism solution in the updated structure map [21] (b) North cluster (top) and south cluster (bottom) focal mechanism.

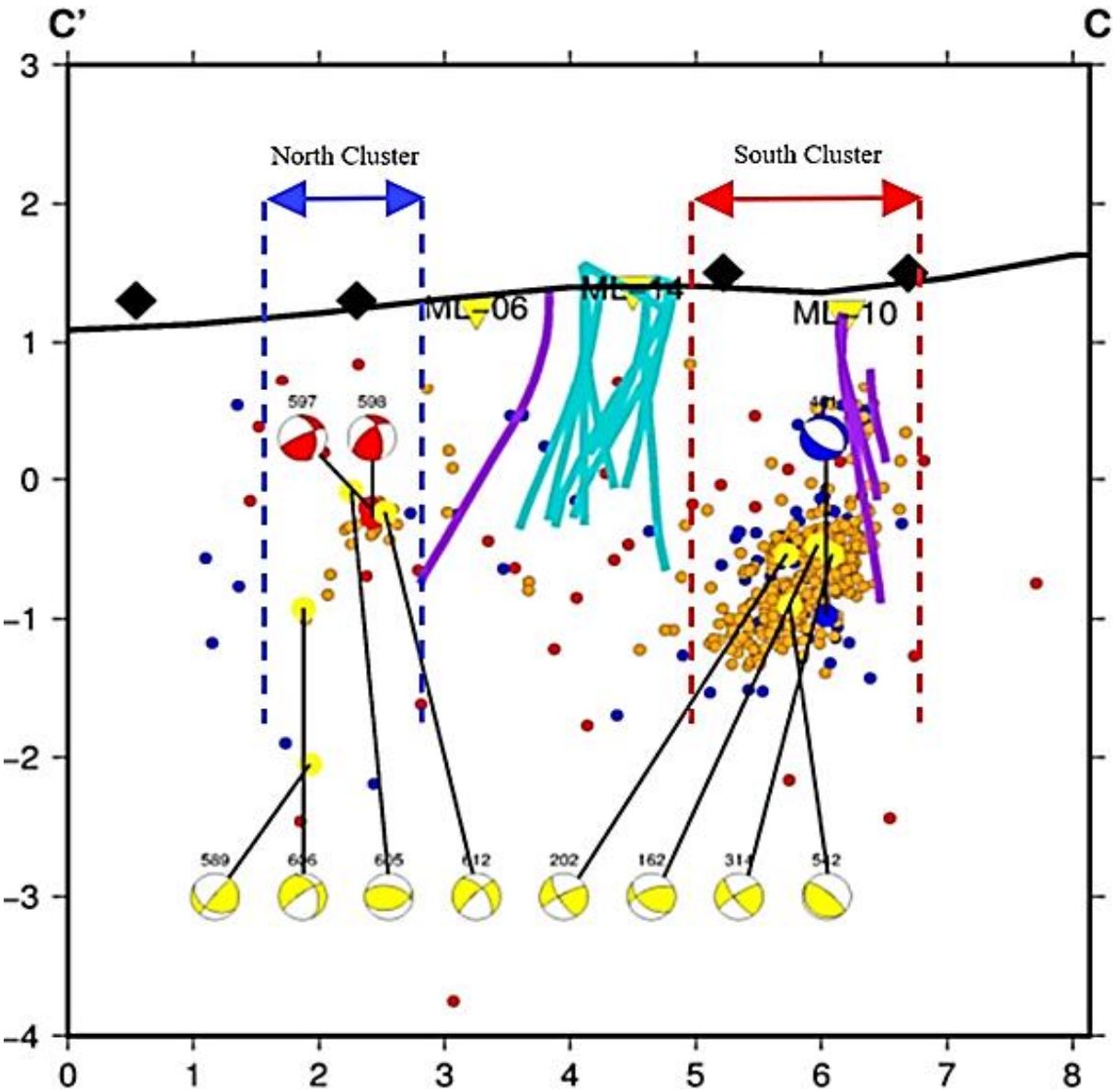

Figure 10. Vertical sections of focal mechanism solutions in Muara Laboh geothermal field, both North cluster and South cluster. Normal fault (yellow beach ball), strike slip (red beach ball), and thrust fault (blue beach ball).

7. Kinematic

The kinematic of the geology structures base on focal mechanism at Muara Laboh geothermal field is shown in Figure 11. In brief, the focal mechanisms support the kinematics of structures form in a pull apart basin where the movement of these strike slip faults resulted in generation of step over NE-SW normal faults, suggesting that extensional regime is indeed controlling the southern area during the reinjection as the faults are reactivated. These step over faults also observed by the magnetotelluric (MT) and microgravity data [21].

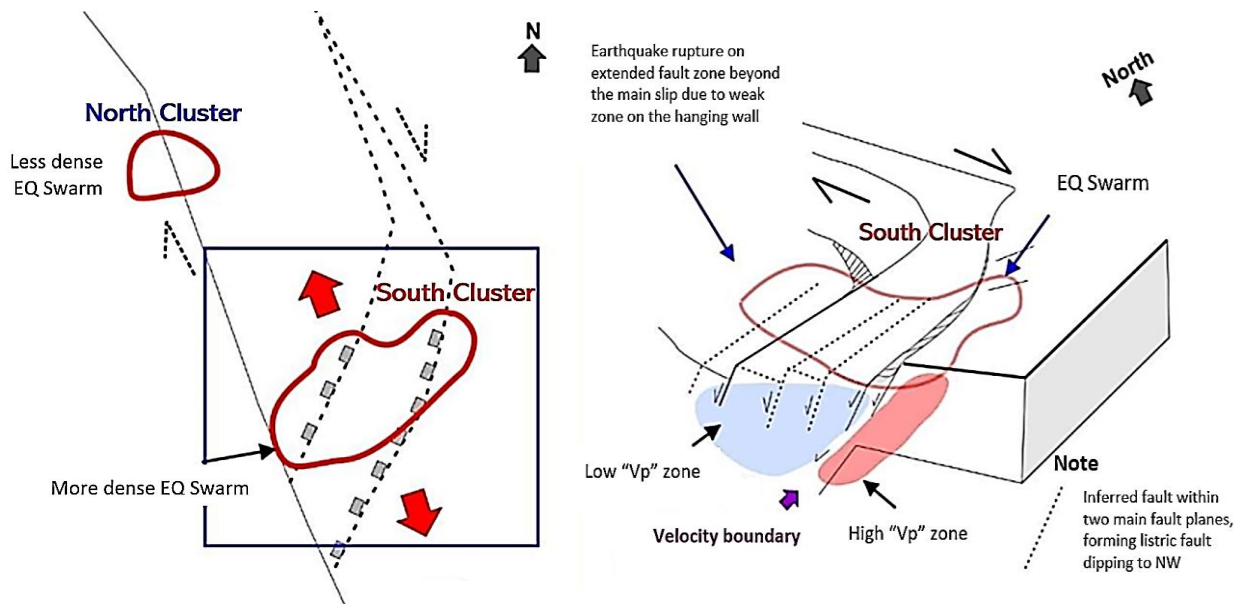

Figure 11. The kinematic of geology structures based on focal mechanism at Muara Laboh geothermal field.

8. Conclusion

Microseismic monitoring has been done for 383 days continuously started from November 13th, 2019 to November 30th, 2020 in Muara Laboh geothermal field owned by PT Supreme Energy Muara Laboh (SEML). Based on the results obtained in this study, below are following conclusions:

1. The accuracy of the hypocenter was improved using waveform cross-correlation (WCC) technique;
2. The Double Difference (DD) was successfully relocate the hypocenter and further improve the accuracy of the events location;
3. Moment magnitude (Mw) ranges between -0.5 to 2 with the magnitude of completeness 0.16;
4. The distribution of focal mechanism solutions shows that most of event has normal fault component suggesting that extensional regime is indeed controlling the area during the reinjection round as the faults are reactivated.
5. Kinematic model for the Muara Laboh geothermal field can be explained as below:
   a. The South cluster of microseismic swarm is denser than those at North cluster and elongate in NEE – SWW direction. The microseismic swarm in this South cluster are restricted with a corridor bounded by two faults striking NE-SW. The swarm are also located beyond two bounding faults, in particular it occurs at the southwest tip within this South cluster;
   b. The controlled microseismic swarm by two NE-SW bounded fault might suggest that the damage zone is existing within the corridor striking parallel with NEE -SWW. This NE-SW bounding fault kinematically a normal fault dipping to the NW (supported by gravity anomaly), this normal movement is controlled by the extensional stress of the NW-SE fault located at the western of Muara Laboh geothermal field.

References

[1] Mussofan, W., Baroek, M.C., Stimac, J., Sidik, R.P., Ramadhan, I., and Santana, S. 2018. Geothermal Resource Exploration along Great Sumatera Fault Segments in Muara Laboh: Perspectives from Geology and Structural Play, *Proceedings, 43rd Workshop on Geothermal Reservoir Engineering*, Stanford University, Stanford, CA

[2] Natawidjaja, D. and Sieh, K. 2000. Neotectonics of the Sumatran Fault, Indonesia, *Journal of Geophysical Research,* Vol. 105, 28, 295 – 28,326

[3] Harris, R., Archuleta, R., and Day, S. 1991. Fault steps and the dynamic rupture process: 2-D numerical simulations of a spontaneously propagating shear fracture, *Geophysical Research Letters*, Vol. 18, 893 – 896
[4] Harris, R. and Day, S. 1993. Dynamics of Fault Interaction: Parallel strike-slip faults, *Journal of Geophysical Research*, Vol. 98, 4461 – 4472
[5] Muraoka, H., Takahashi, M., Sundhoro, H., Dwipa, S., Soeda, Y., Momita, M., and Shimada, K. 2010. Geothermal systems constrained by the sumatran fault and its pull-apart basins in Sumatra, Western Indonesia*, Proceedings, World Geothermal Congress*, Bali, Indonesia
[6] Acocella, V., Bellier, O., Sandri, L., Sebrier, M., and Pramumijoyo, S. 2018. Weak tectono-magmatic relationships along an obliquely convergent plate boundary: Sumatra, Indonesia, *Frontiers of Earth Science*, Vol. 6
[7] Hickman, R.G., Dobson, P.F., van Gerven, M., Sagala, B., and Gunderson, R.P. 2004. Tectonic and stratigraphic evolution of the Sarulla Graben region, North Sumatra, Indonesia, *Journal of Asian Earth Sciences*, Vol. 23, 435 – 448
[8] Satya, D.Y., Soeda, Y., Drakos, P., Astra, D., and Lima Lobato, E.M. 2018. Building a 3D earth model of silangkitang geothermal field, North Sumatra, Indonesia, *Proceedings, 6th International Geothermal Convention and Exhibition*
[9] Pusat Vulkanologi dan Mitigasi Bencana Geologi. 2021. *Tipe Gunung Api di Indonesia (A, B, dan C)*, ESDM website
[10] Havskov, J. and Ottemoller, L. 2010. *Routine Data Processing in Earthquake Seismology*, Springer, 152
[11] Majer, E.L. and Peterson, J. 2007. The impact of injection on seismicity at The Geysers, California Geothermal Field*, International Journal of Rock Mechanics and Mining Sciences*, Vol. 44(8), 1079 – 1090
[12] Wibowo, D.A.S., Nordquist, G.A., Stimac, J., and Suminar, A. 2010. Monitoring Microseismicity during Well Stimulation at the Salak Geothermal Field, Indonesia, *Proceedings*, *World Geothermal Congress*, Bali, Indonesia
[13] Simiyu, S.M. and Keller, G.R. 2000. Seismic monitoring of the Olkaria Geothermal area, Kenya Rift valley, *Journal of Volcanology and Geothermal Research*, Vol. 95, 197 – 208
[14] Majer, E.L., Baria, R., Stark, M., Oates, S., Bommer, J., Smith, B., and Asanuma, H. 2007. Induced Seismicity associated with Enhanced Geothermal Systems*, Geothermics*, Vol. 36, 185 – 222
[15] Ardianto, A., Husni, Y., Nugraha, A., Muzli, M., Zulfakriza, Z., Afif, H., Sahara, D.P., Widiyantoro, S., Priyono, A., and Puspito, N.T. 2019. Implementation of Filter Picker Algorithm for Aftershock Identification of Lombok Earthquake 2018, *Jurnal Geofisika*, Vol. 17, 25 – 31
[16] Lomax, A., Satriano, C., and Vasallo, M. 2012. Automatic Picker Developments and Optimization: FilterPicker-a Robust, Broadband Picker for Real-Time Seismic Monitoring and Earthquake Early Warning, *Seismological Research Letters,* Vol. 83, 531 – 540
[17] Waldhauser, F. and Ellsworth, W.L. 2000. A double-difference earthquake location algorithm: Method and application to the Northern Hayward fault, California, *Bulletin of the Seismological Society of America*, Vol. 90, 1353 – 1368
[18] Boore, D. and Boatwright, J. 1984. Average body-wave correction coefficient, *Bulletin Seismological Society America*, Vol. 74, 1615 – 1621
[19] Stork, A.L., Verdon, J.P., and Kendall, J.M. 2014. The robustness of seismic moment and magnitudes estimated using spectral analysis, *Geophysical Prospecting*, Vol. 62, 862 – 878
[20] Maxwell, S. 2014. *Microseismic imaging of hydraulic fracturing: Improved engineering of unconventional shale reservoirs*, Publication of SEG
[21] SEML 2021. *Muara Laboh Reservoir Monitoring and Static Model Update*, Presentation Slide, Unpublished